

ONLINE APPENDIX TO

A Hundred Years of Business Cycles and the Phillips curve

Lapo Bini¹, Lucrezia Reichlin², and Giovanni Ricco³

¹UC San Diego

²London Business School, Now-Casting Economics, and CEPR

³École Polytechnique CREST, University of Warwick, OFCE-SciencesPo, and CEPR

August 5, 2024

Abstract

This Online Appendix provides the estimation procedure and all the charts for each the models described in ‘A Hundred Years of Business Cycles and the Phillips curve’.

JEL classification: X11.

Keywords: Phillips Curve, Semi-structural models.

Contents

A Additional results	2
A.1 Baseline model, sample 1900-2019	2
A.2 Baseline model, sample 1960/2019	6
A.3 Model with oil prices, FFR not responding to oil, sample 1960-2019	10
A.4 Model with oil prices, FFR not responding to oil, sample 1960-2019	14
A.5 The extended COVID sample	18
B Stability of the model	22
C Rolling windows	27
D Adaptive Metropolis-Within-Gibbs	28
D.1 Algorithm	28

A Additional results

A.1 Baseline model, sample 1900-2019

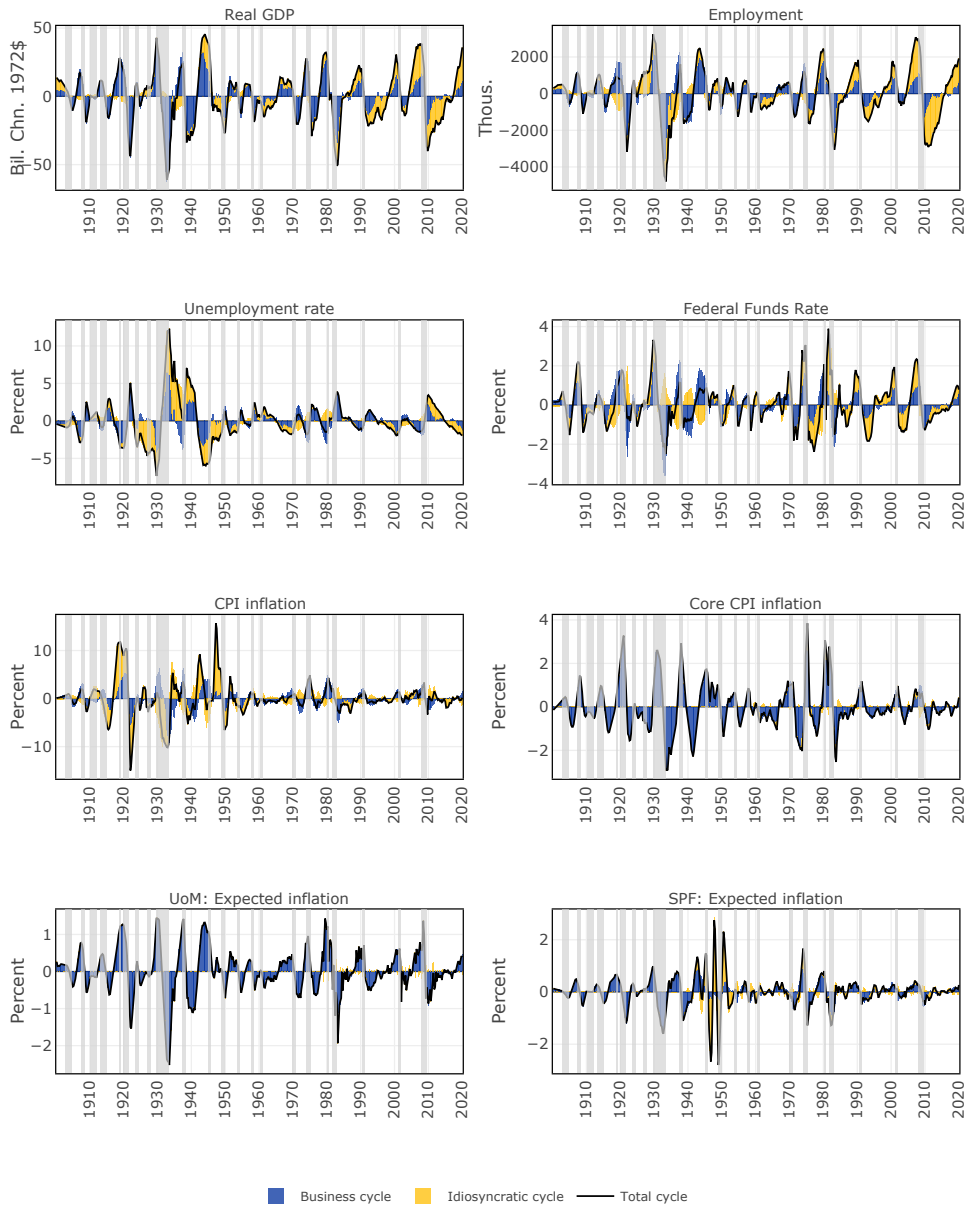


Figure 1: Historical decomposition of the cycles, as estimated by the model. The chart reports the business cycle (in blue), and idiosyncratic cycle (in yellow). The model is estimated over the sample 1900-2019.

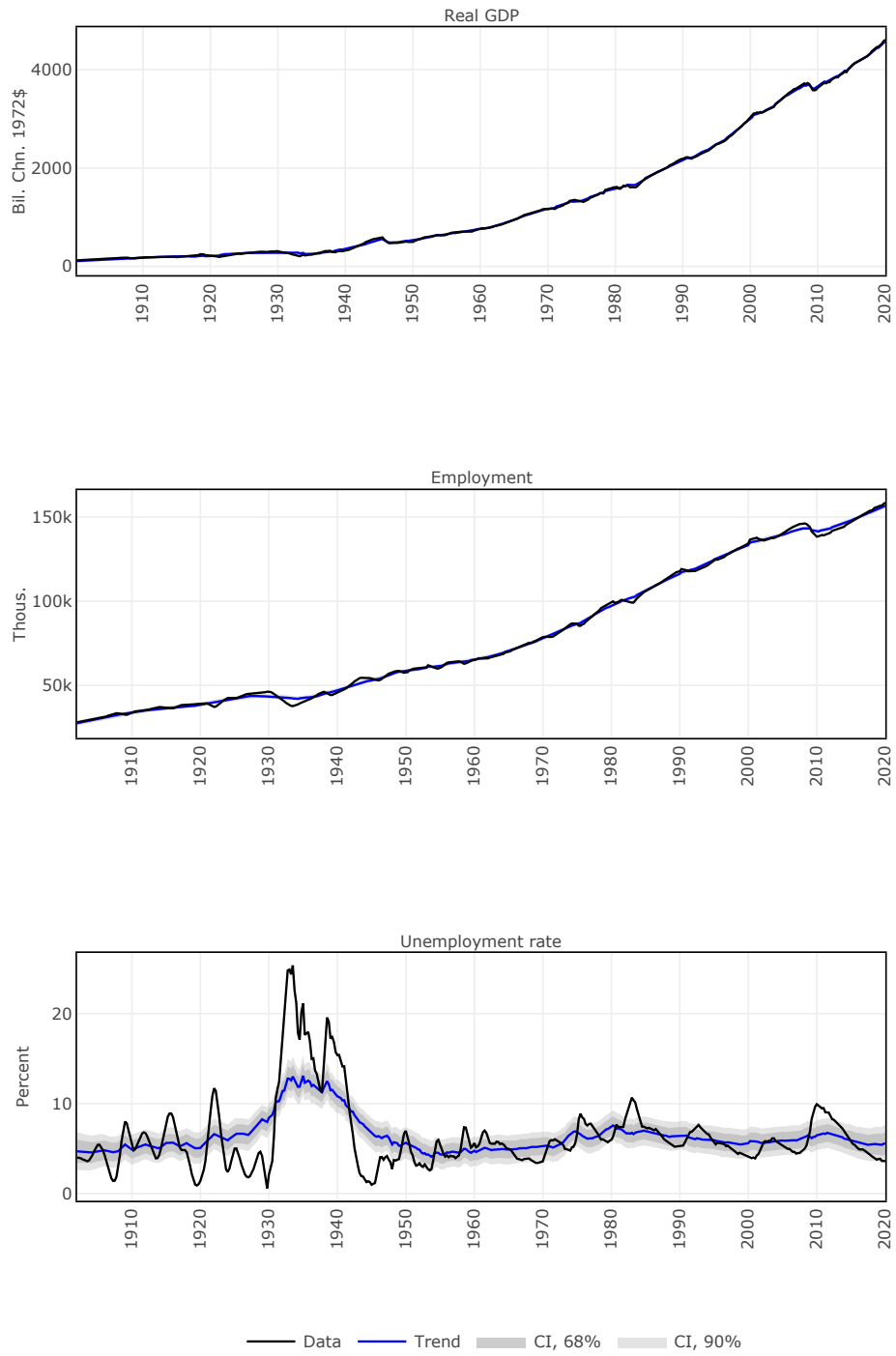


Figure 2: Independent trends of output, employment, unemployment, and oil prices (in blue), with coverage intervals at 68% coverage (dark shade) and 90% coverage (light shade), as estimated by the model. The model is estimated over the sample 1900-2019.

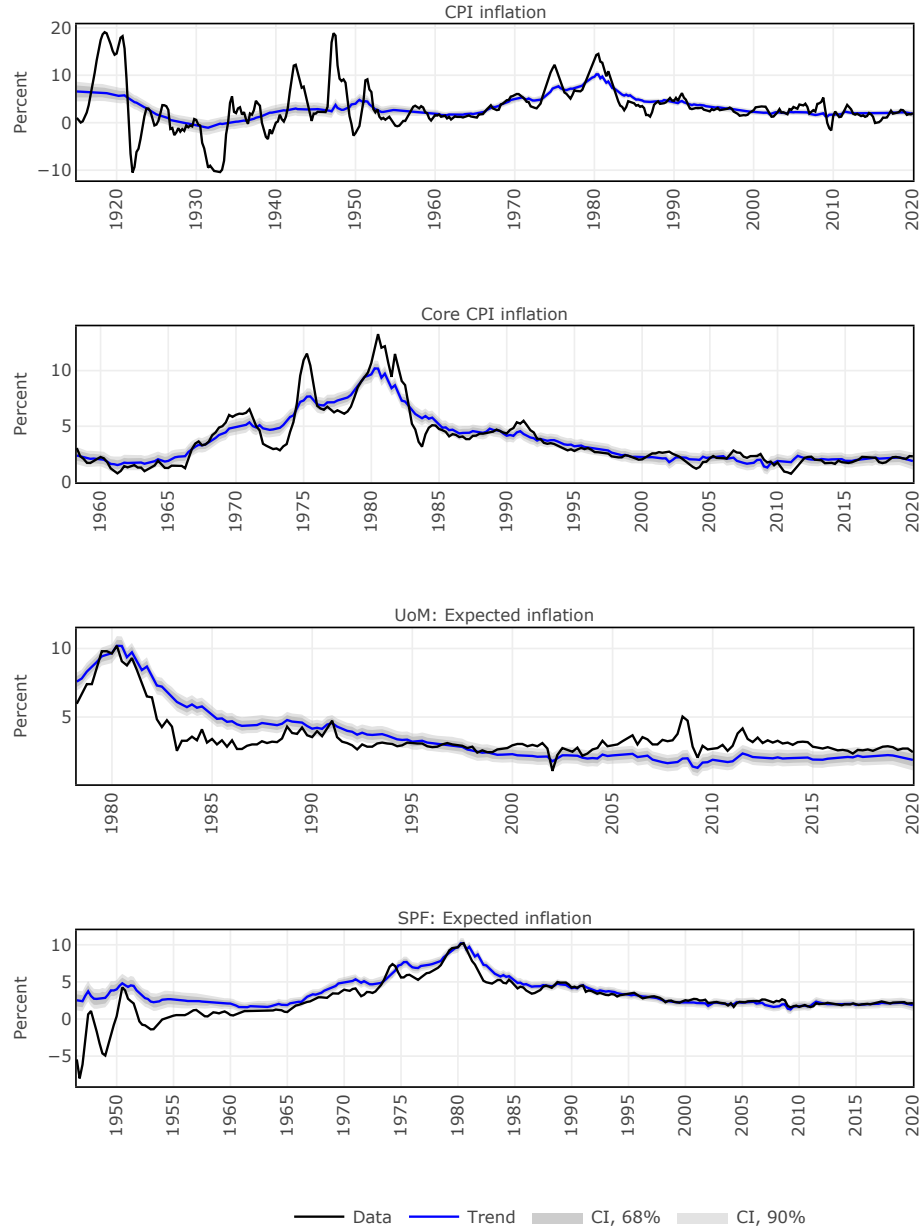


Figure 3: Trend common to CPI inflation, core CPI inflation, and inflation expectations (in blue), with coverage intervals at 68% coverage (dark shade) and 90% coverage (light shade), as estimated by the model. The model is estimated over the sample 1900-2019.

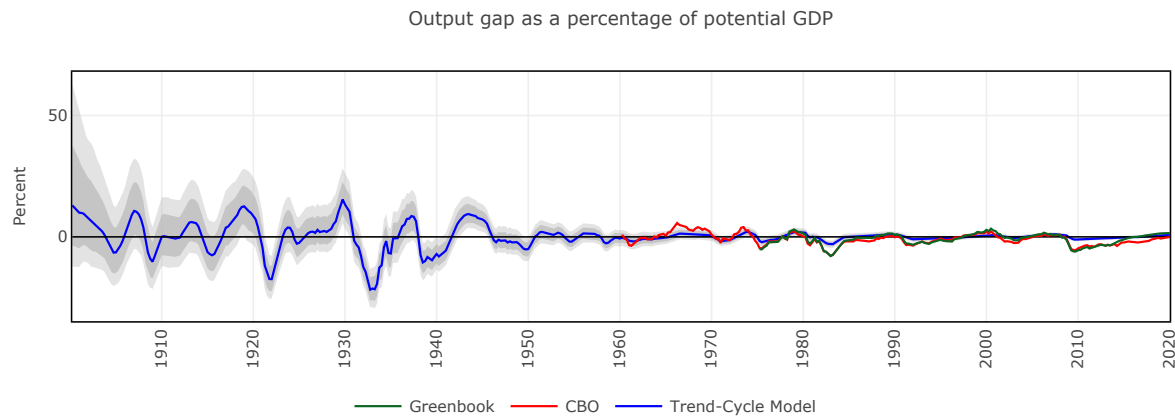


Figure 4: Output gap

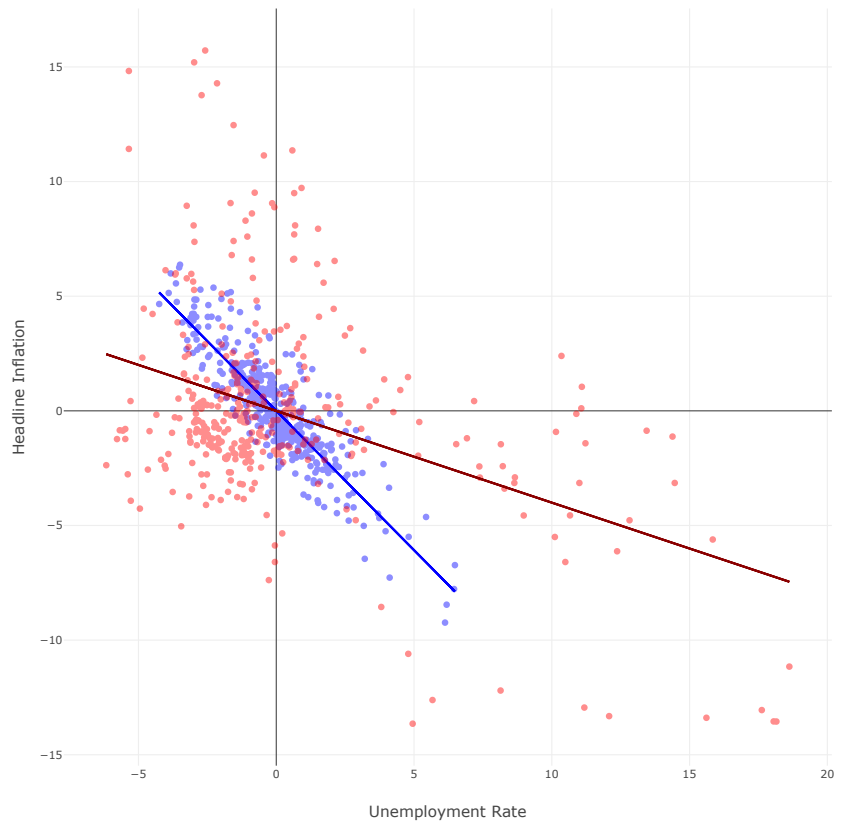


Figure 5: This chart plots the business cycle component of CPI inflation against the business cycle component of the unemployment rate (blue dots) and the corresponding bivariate linear regression line (blue line). The chart also plots demeaned CPI inflation against the demeaned unemployment rate (red dots) and the corresponding bivariate linear regression line (red line).

A.2 Baseline model, sample 1960/2019

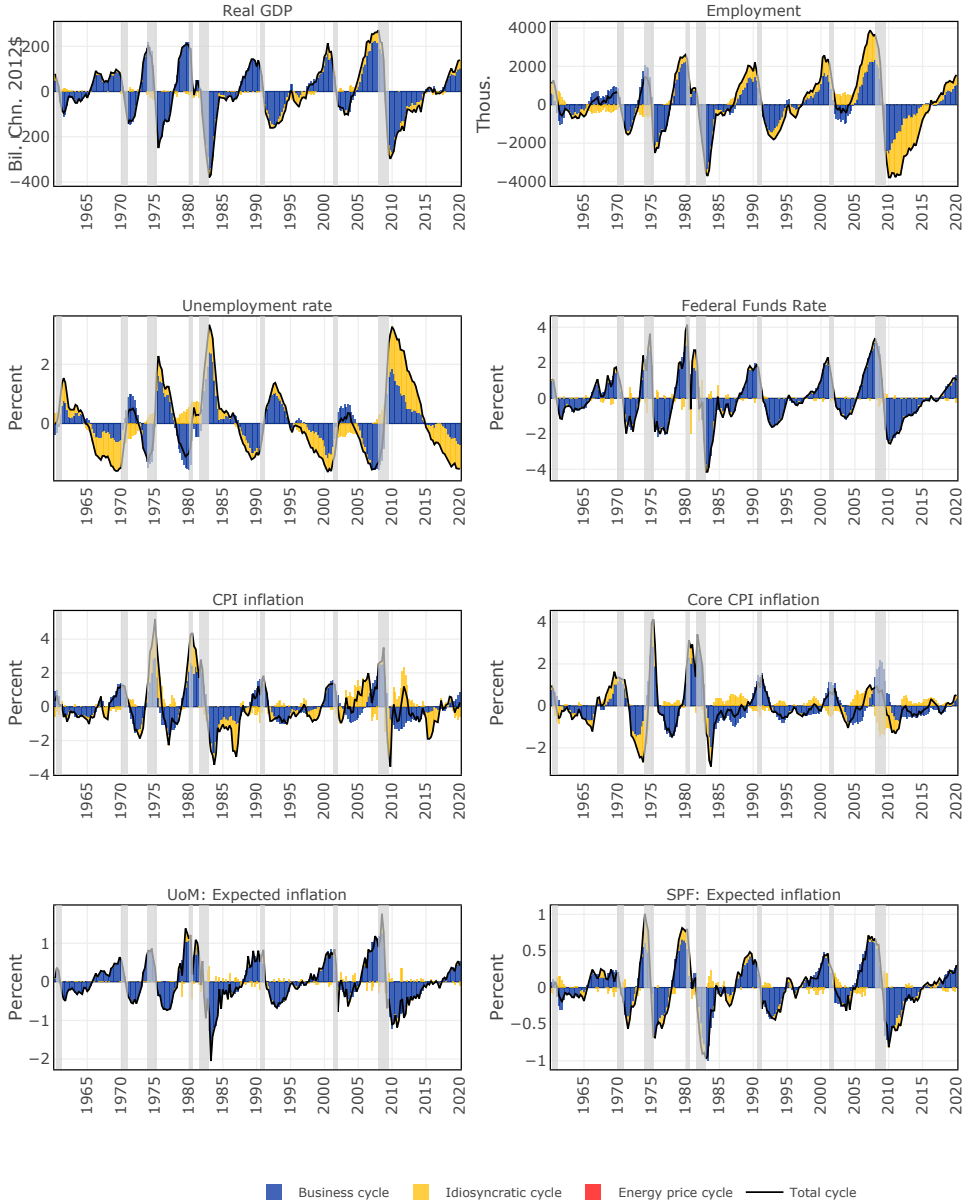


Figure 6: Historical decomposition of the cycles, as estimated by the model. The chart reports the business cycle (in blue), and idiosyncratic cycle (in yellow). The model is estimated over the sample 1960-2019.

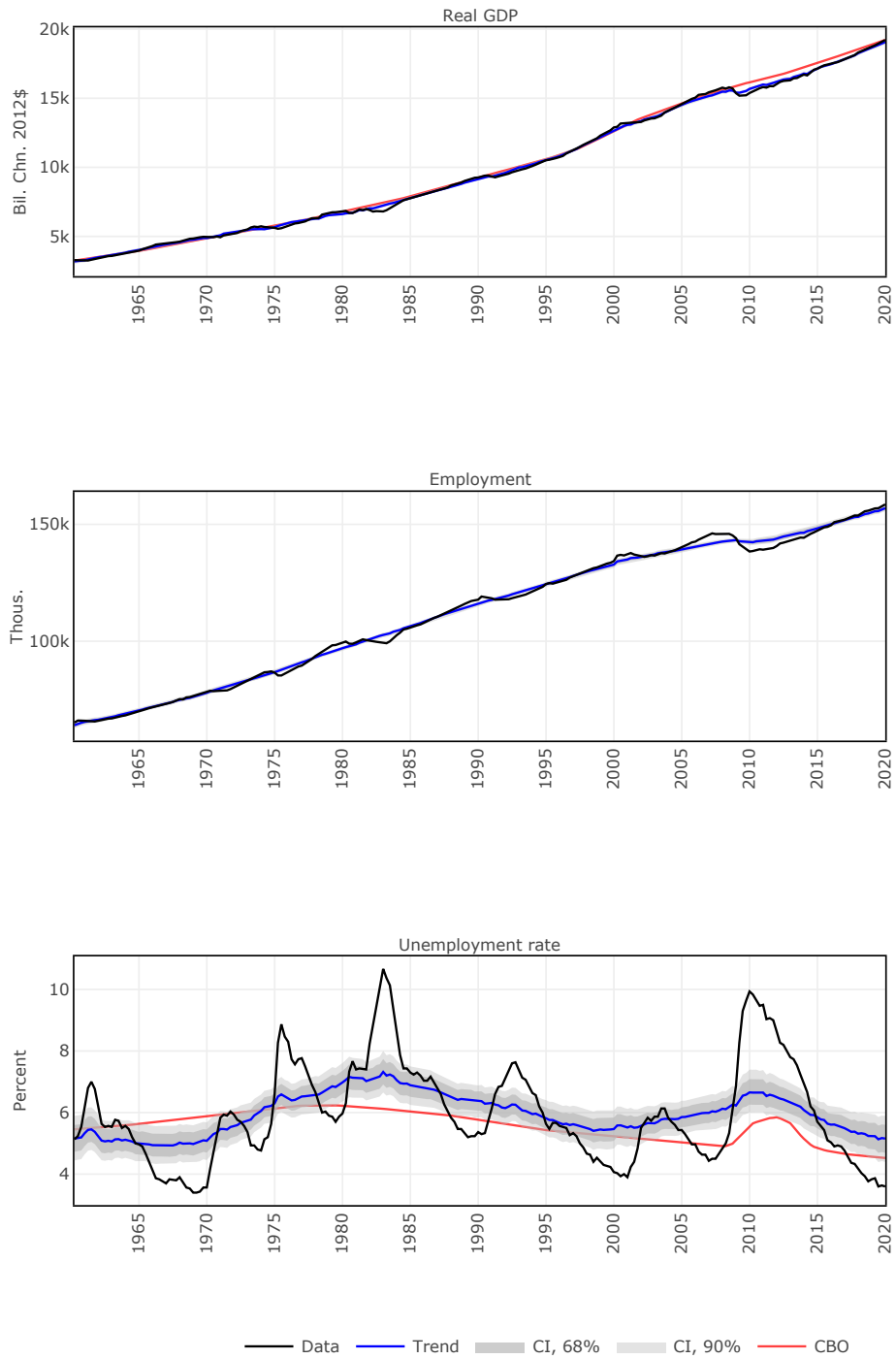


Figure 7: Independent trends of output, employment, unemployment, and oil prices (in blue), with coverage intervals at 68% coverage (dark shade) and 90% coverage (light shade), as estimated by the model. The model is estimated over the sample 1960-2019.

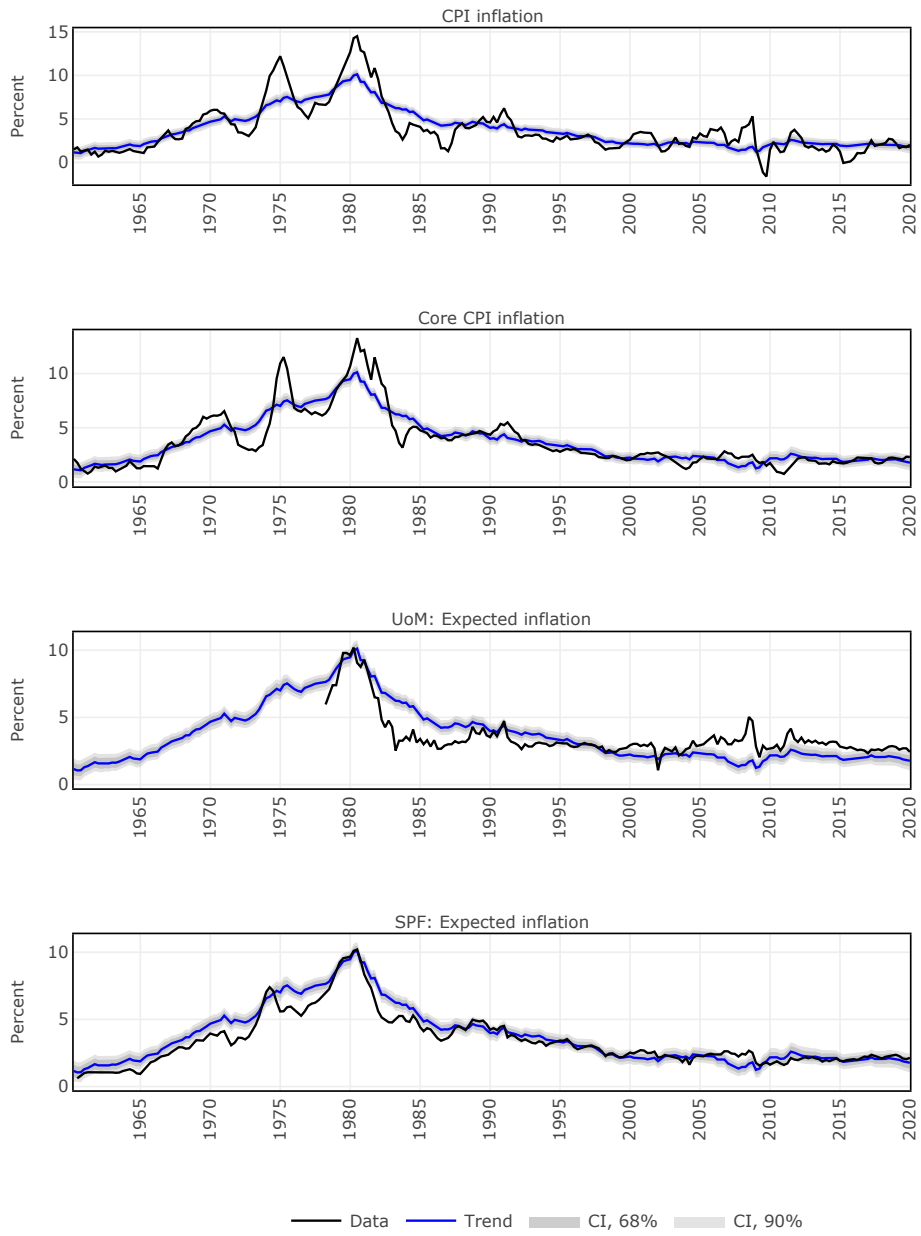


Figure 8: Trend common to CPI inflation, core CPI inflation, and inflation expectations (in blue), with coverage intervals at 68% coverage (dark shade) and 90% coverage (light shade), as estimated by the model. The model is estimated over the sample 1960-2019.

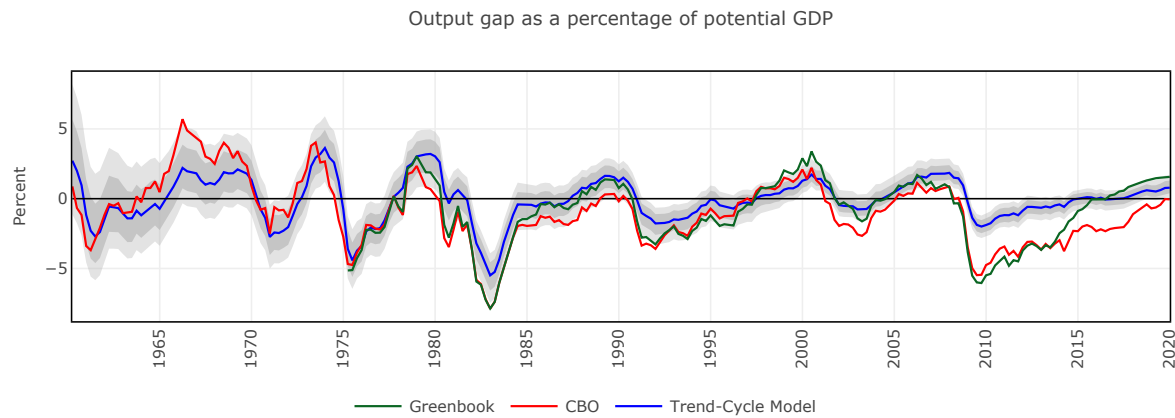


Figure 9: Output gap

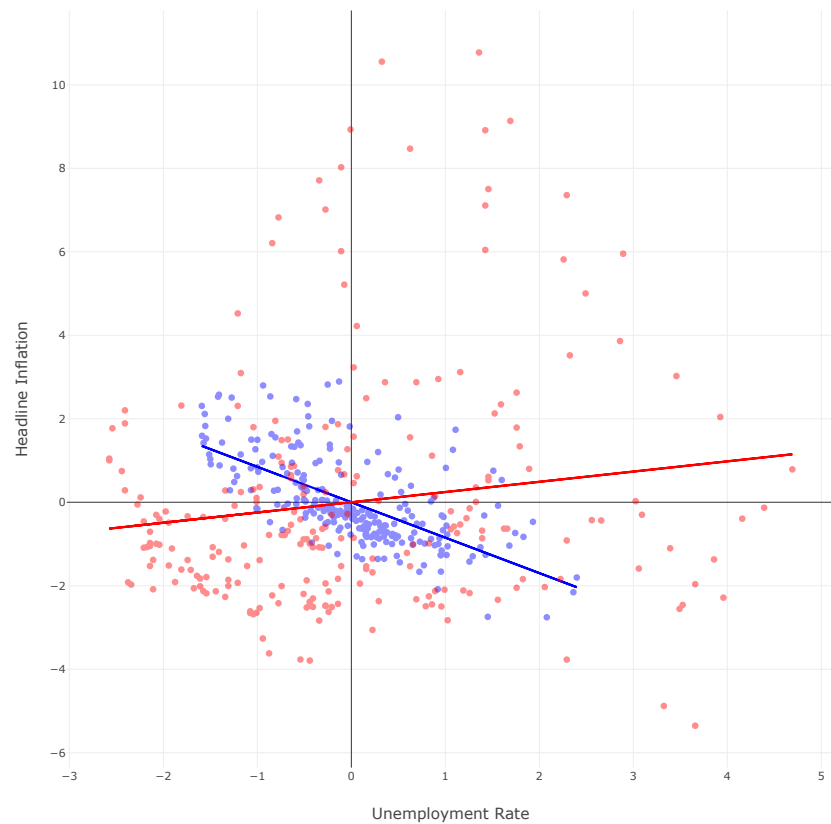


Figure 10: This chart plots the business cycle component of CPI inflation against the business cycle component of the unemployment rate (blue dots) and the corresponding bivariate linear regression line (blue line). The chart also plots demeaned CPI inflation against the demeaned unemployment rate (red dots) and the corresponding bivariate linear regression line (red line).

A.3 Model with oil prices, FFR not responding to oil, sample 1960-2019

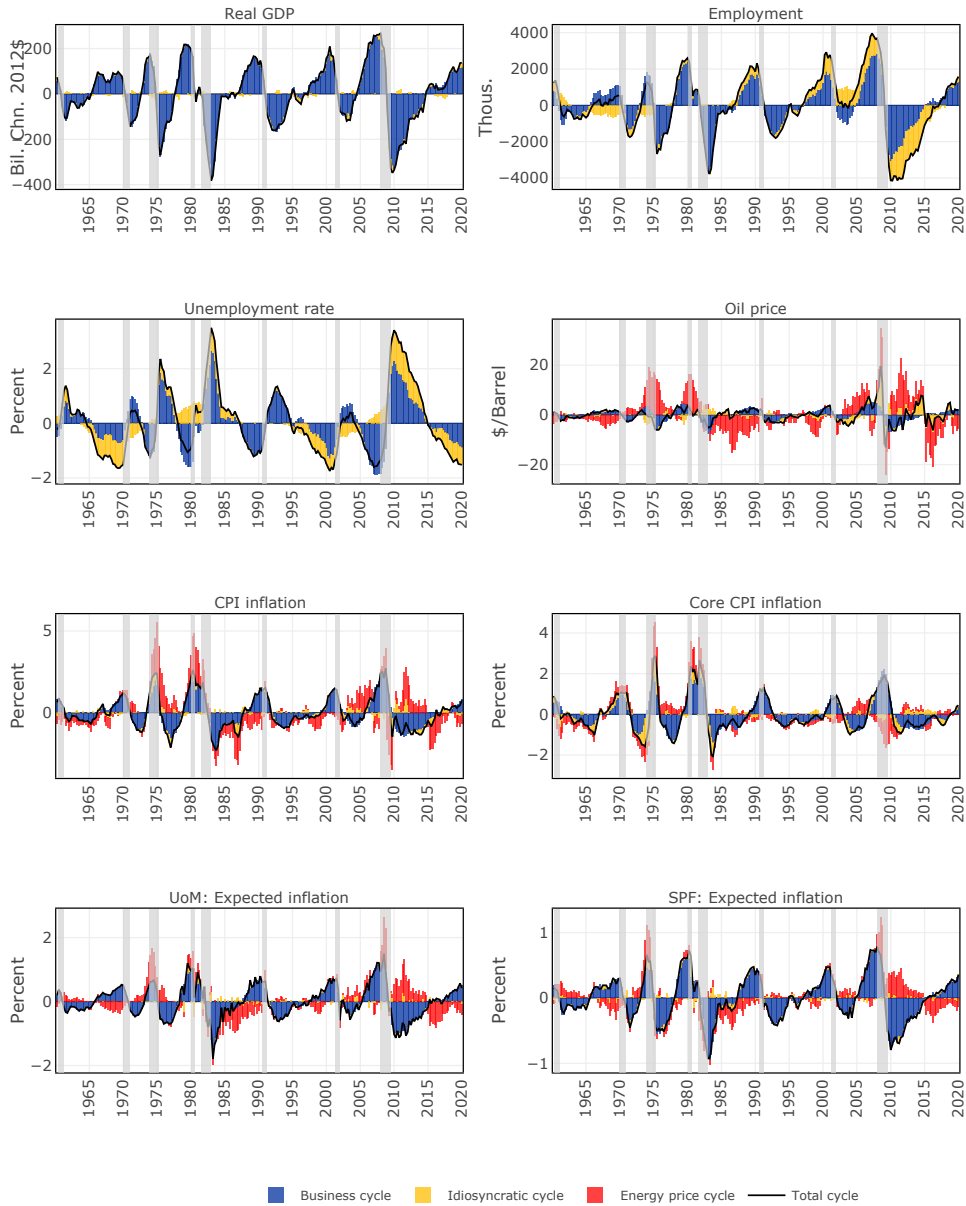


Figure 11: Historical decomposition of the cycles, as estimated by the model. The chart reports the business cycle (in blue), and idiosyncratic cycle (in yellow). The model is estimated over the sample 1960-2019.

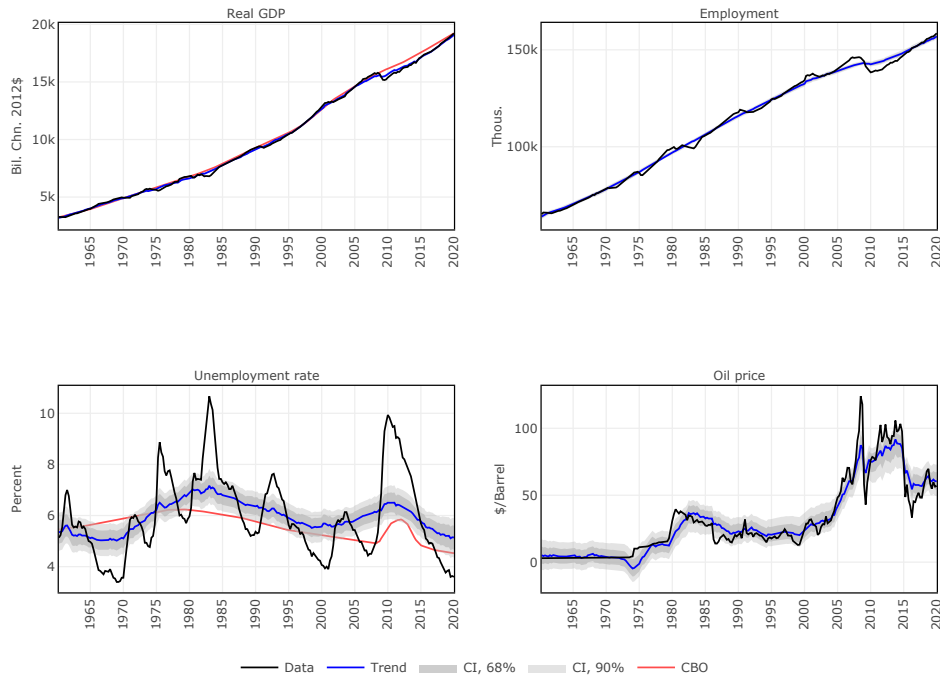


Figure 12: Independent trends of output, employment, unemployment, and oil prices (in blue), with coverage intervals at 68% coverage (dark shade) and 90% coverage (light shade), as estimated by the model. The model is estimated over the sample 1960-2019.

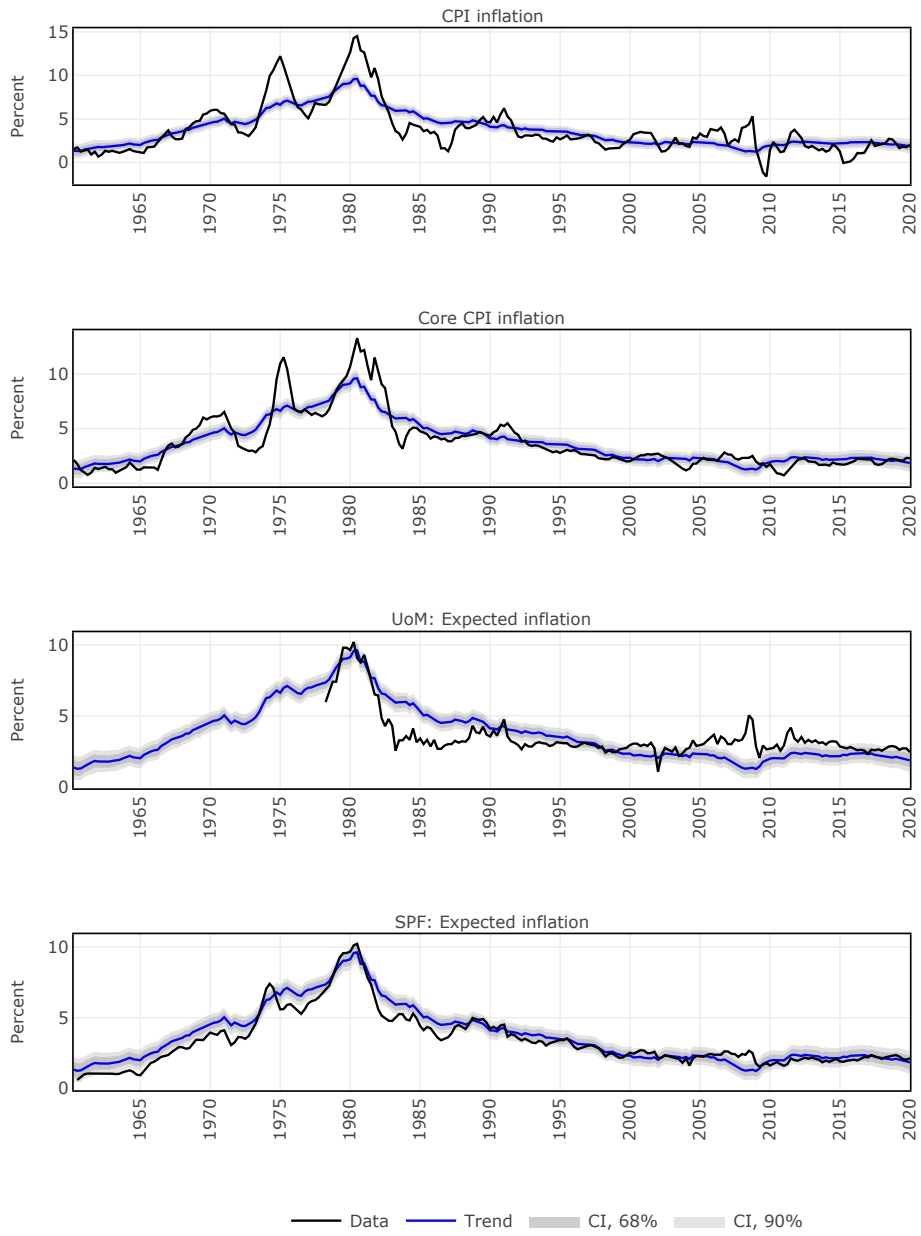


Figure 13: Trend common to CPI inflation, core CPI inflation, and inflation expectations (in blue), with coverage intervals at 68% coverage (dark shade) and 90% coverage (light shade), as estimated by the model. The model is estimated over the sample 1960-2019.

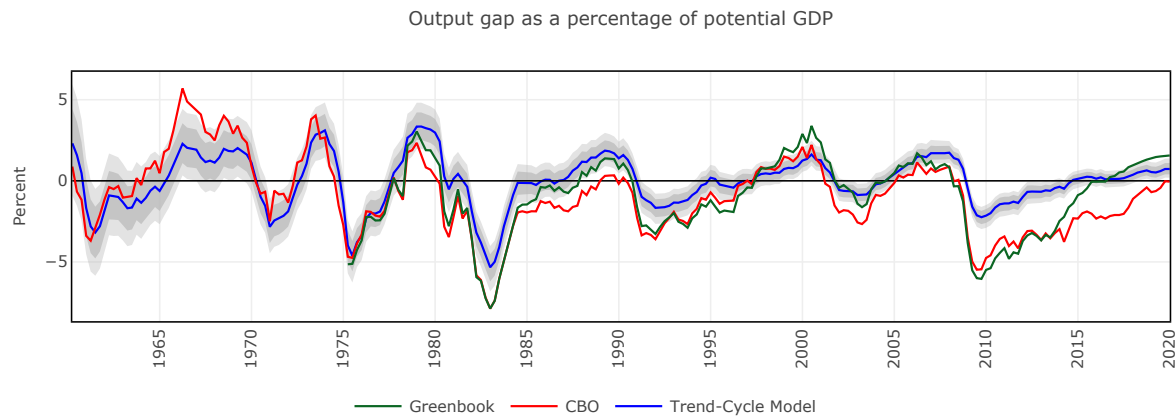


Figure 14: Output gap

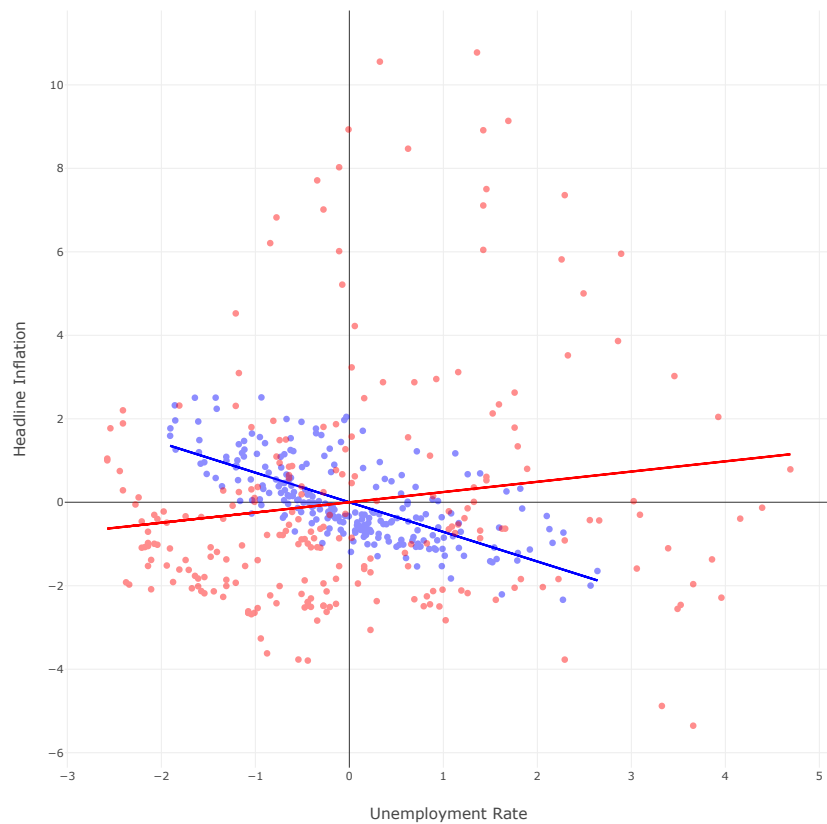


Figure 15: This chart plots the business cycle component of CPI inflation against the business cycle component of the unemployment rate (blue dots) and the corresponding bivariate linear regression line (blue line). The chart also plots demeaned CPI inflation against the demeaned unemployment rate (red dots) and the corresponding bivariate linear regression line (red line).

A.4 Model with oil prices, FFR not responding to oil, sample 1960-2019

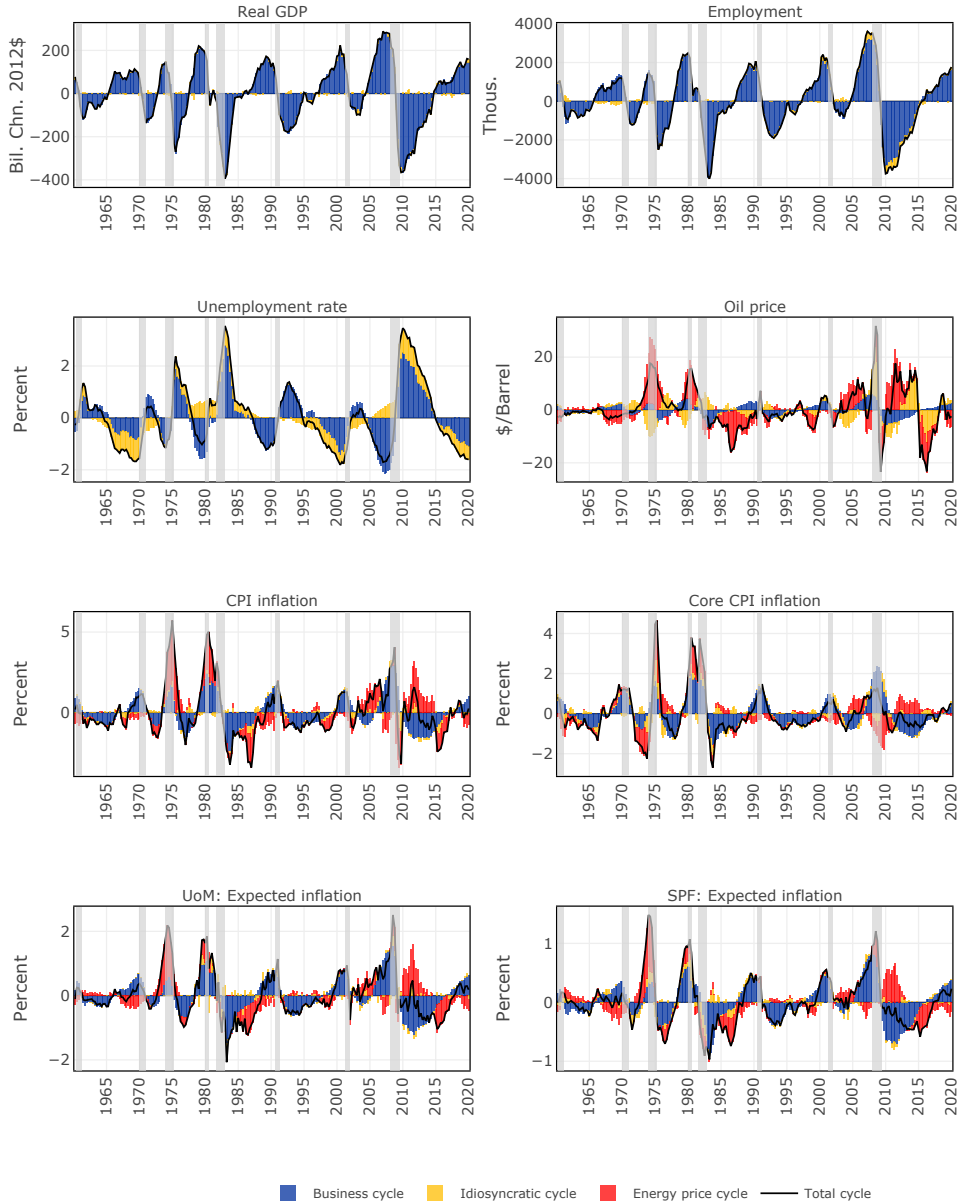


Figure 16: Historical decomposition of the cycles, as estimated by the model. The chart reports the business cycle (in blue), Energy price cycle (in red), and idiosyncratic cycle (in yellow). The model is estimated over the sample 1960-2019.

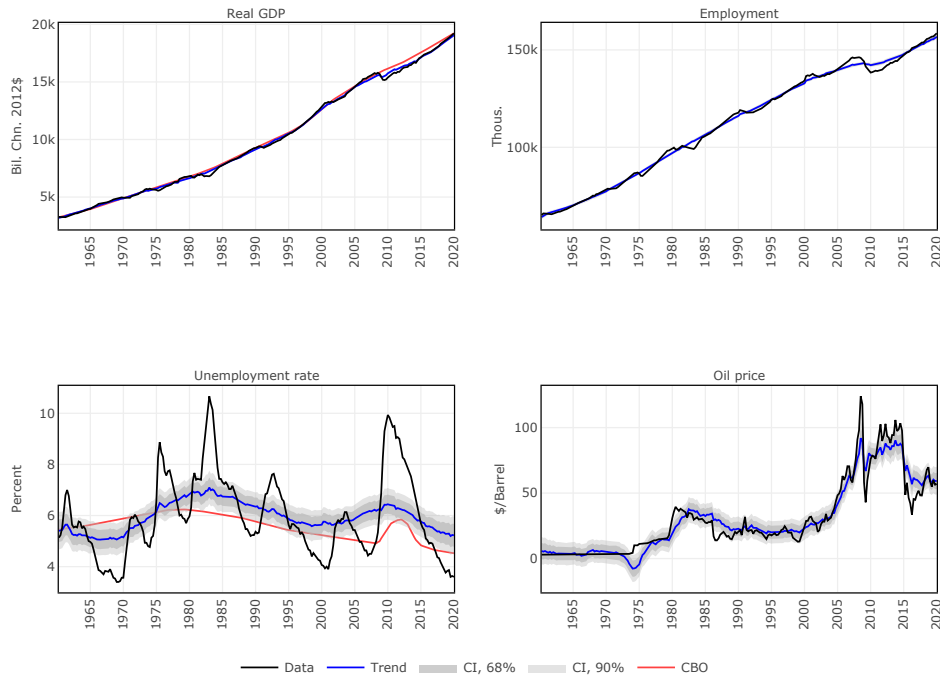


Figure 17: Independent trends of output, employment, unemployment, and oil prices (in blue), with coverage intervals at 68% coverage (dark shade) and 90% coverage (light shade), as estimated by the model. The model is estimated over the sample 1960-2019.

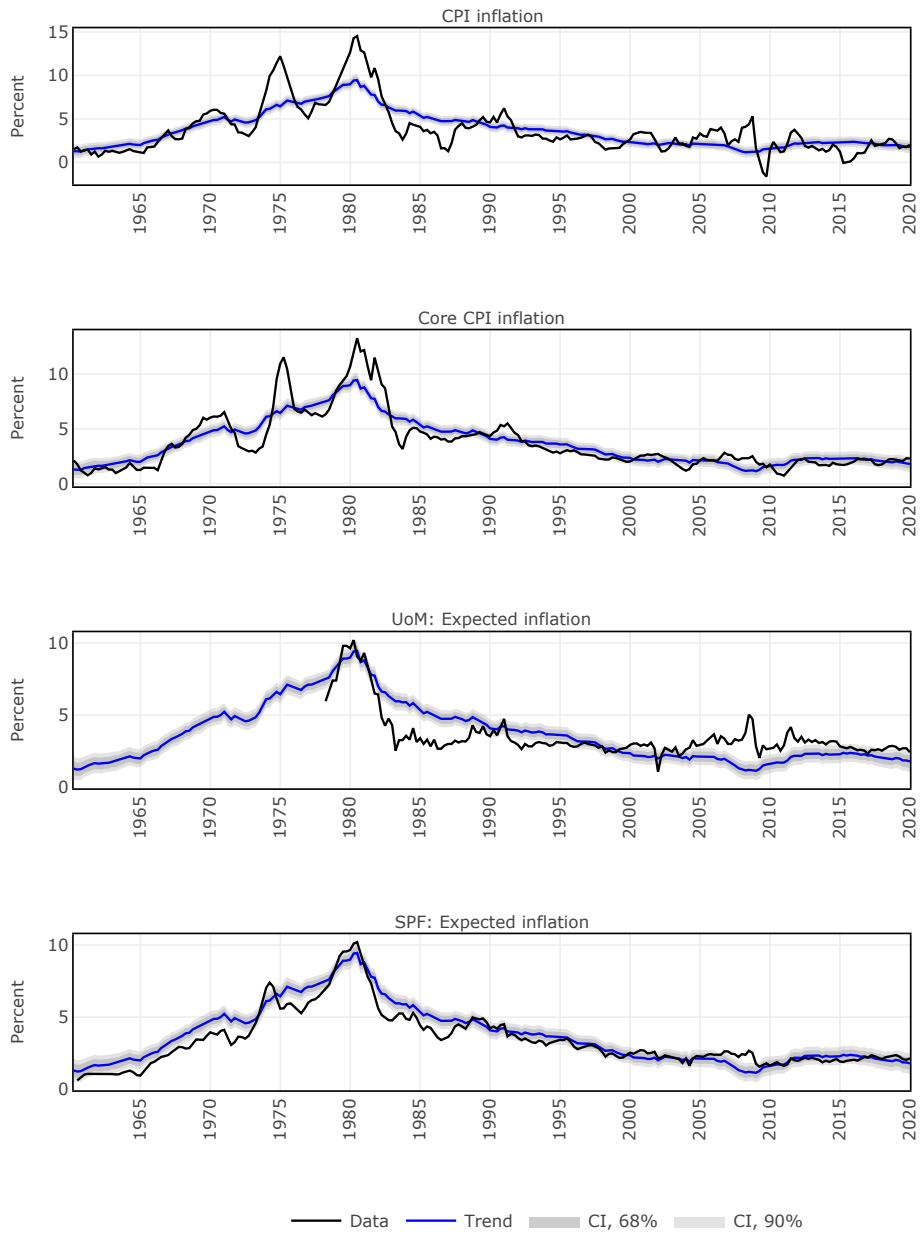


Figure 18: Trend common to CPI inflation, core CPI inflation, and inflation expectations (in blue), with coverage intervals at 68% coverage (dark shade) and 90% coverage (light shade), as estimated by the model. The model is estimated over the sample 1960-2019.

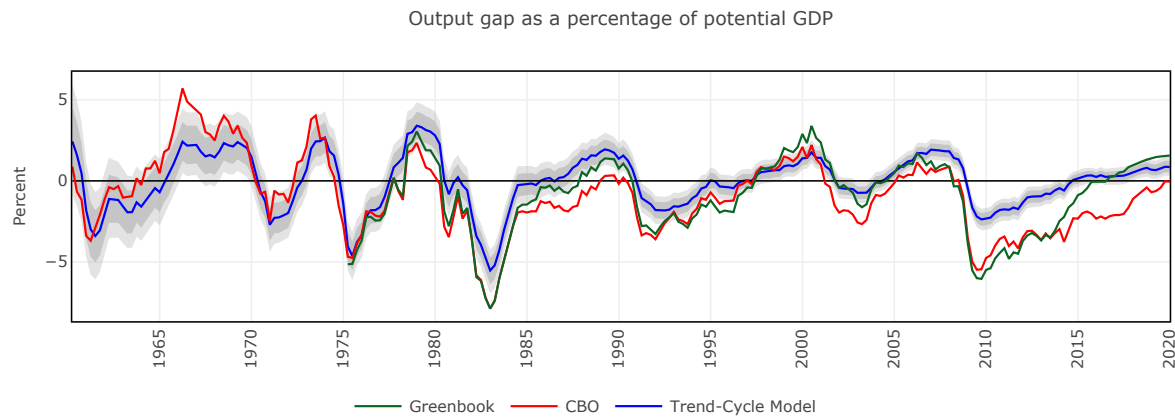


Figure 19: Output gap

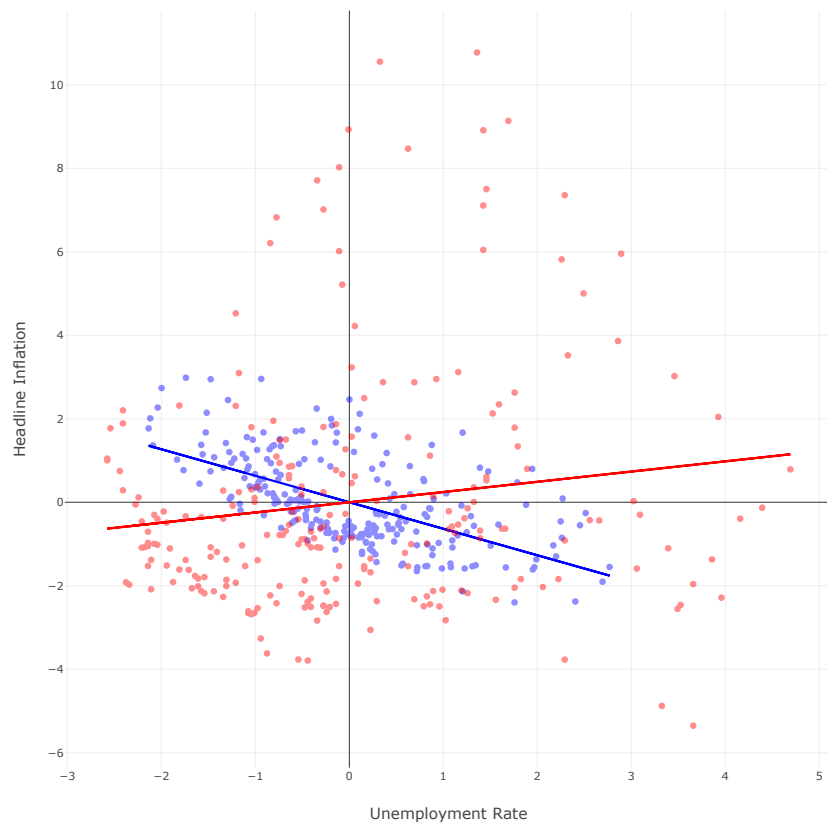


Figure 20: This chart plots the business cycle component of CPI inflation against the business cycle component of the unemployment rate (blue dots) and the corresponding bivariate linear regression line (blue line). The chart also plots demeaned CPI inflation against the demeaned unemployment rate (red dots) and the corresponding bivariate linear regression line (red line).

A.5 The extended COVID sample

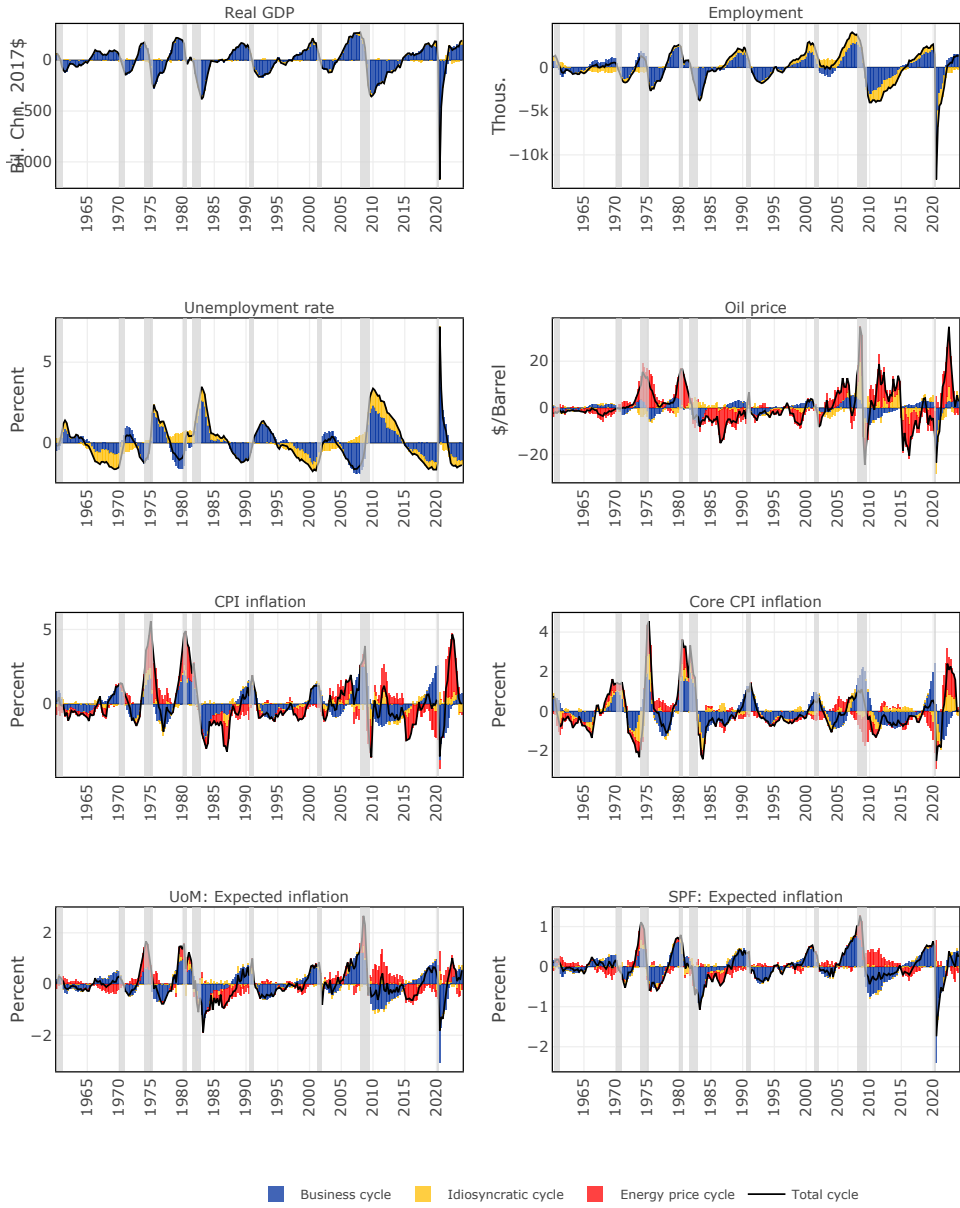


Figure 21: Historical decomposition of the cycles, as estimated by the model. The chart reports the business cycle (in blue), and idiosyncratic cycle (in yellow). The model is estimated over the sample 1960-2019.

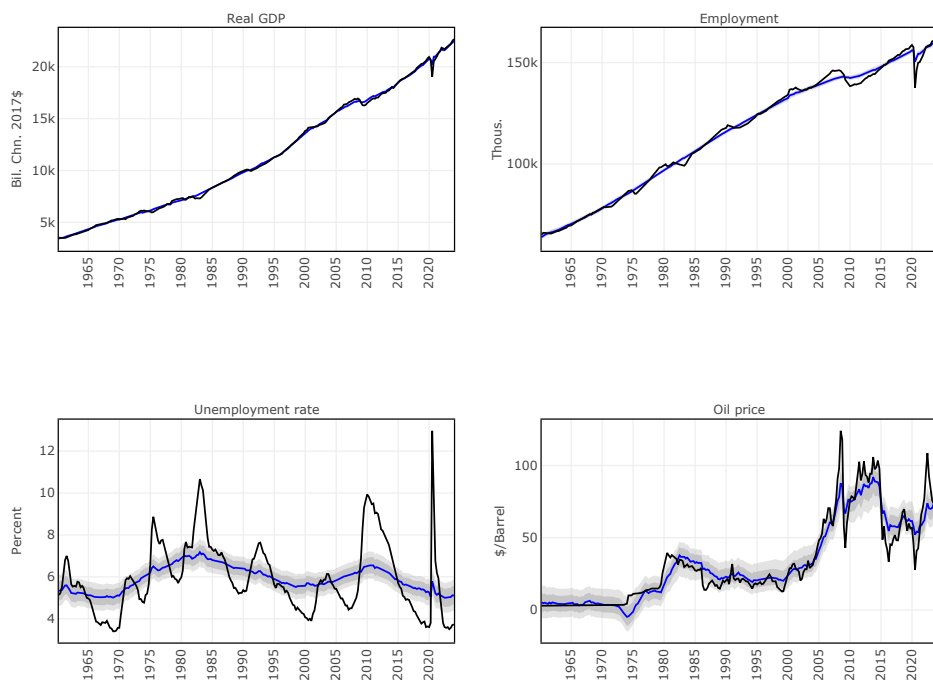


Figure 22: Independent trends of output, employment, unemployment, and oil prices (in blue), with coverage intervals at 68% coverage (dark shade) and 90% coverage (light shade), as estimated by the model. The model is estimated over the sample 1960-2019.

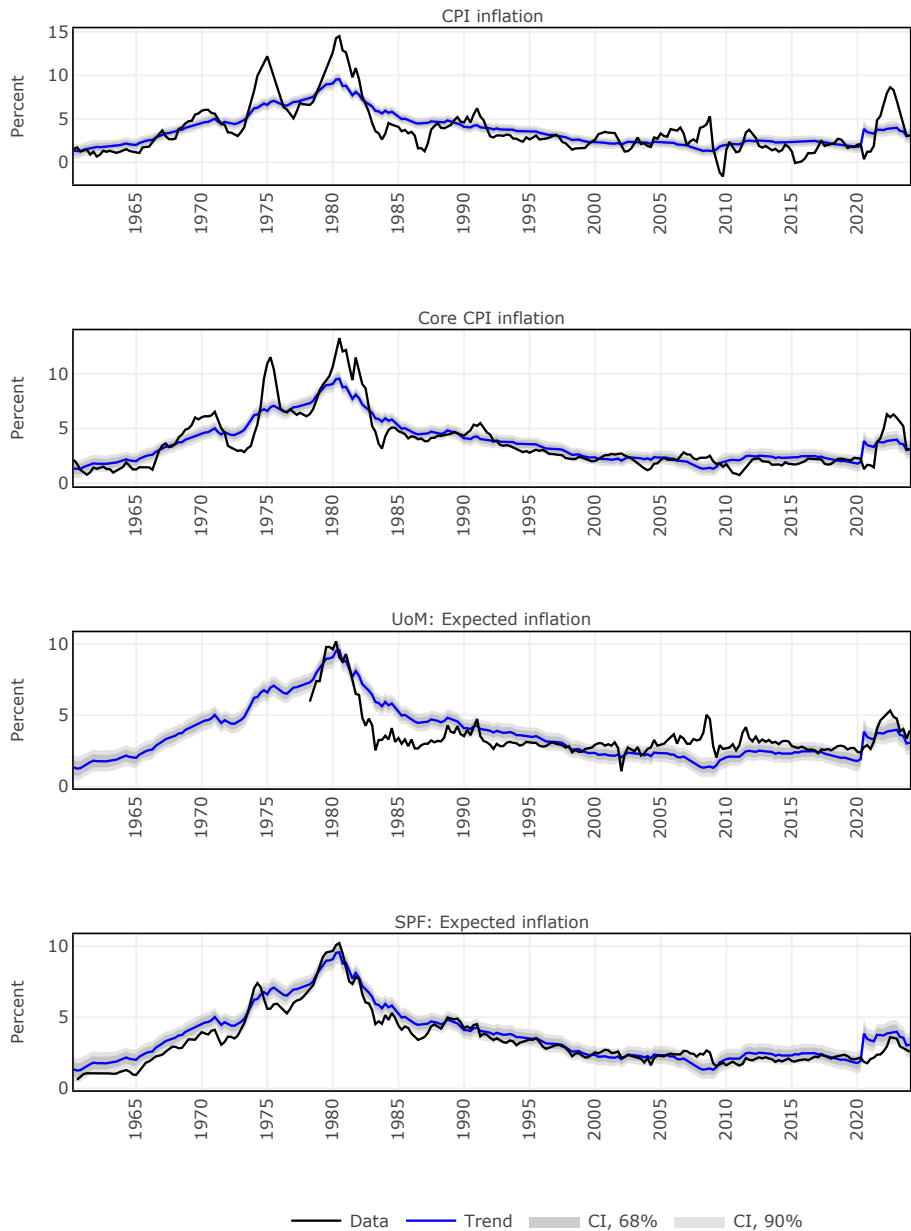


Figure 23: Trend common to CPI inflation, core CPI inflation, and inflation expectations (in blue), with coverage intervals at 68% coverage (dark shade) and 90% coverage (light shade), as estimated by the model. The model is estimated over the sample 1960-2019.

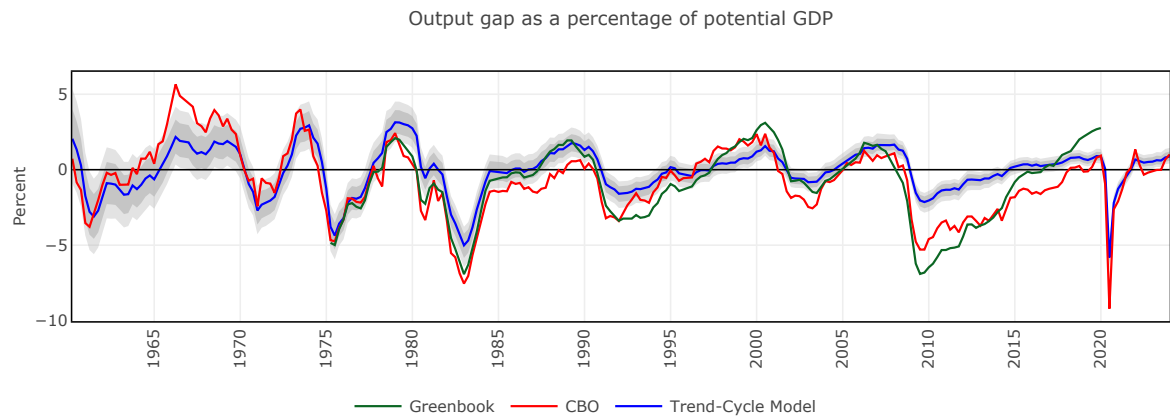


Figure 24: Output gap

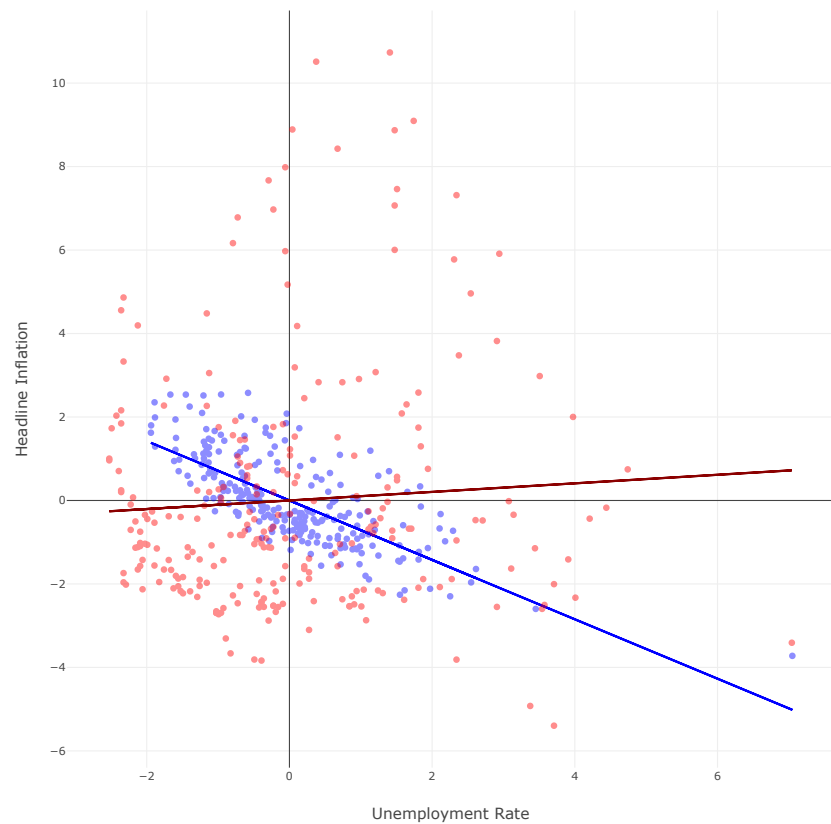


Figure 25: This chart plots the business cycle component of CPI inflation against the business cycle component of the unemployment rate (blue dots) and the corresponding bivariate linear regression line (blue line). The chart also plots demeaned CPI inflation against the demeaned unemployment rate (red dots) and the corresponding bivariate linear regression line (red line).

B Stability of the model

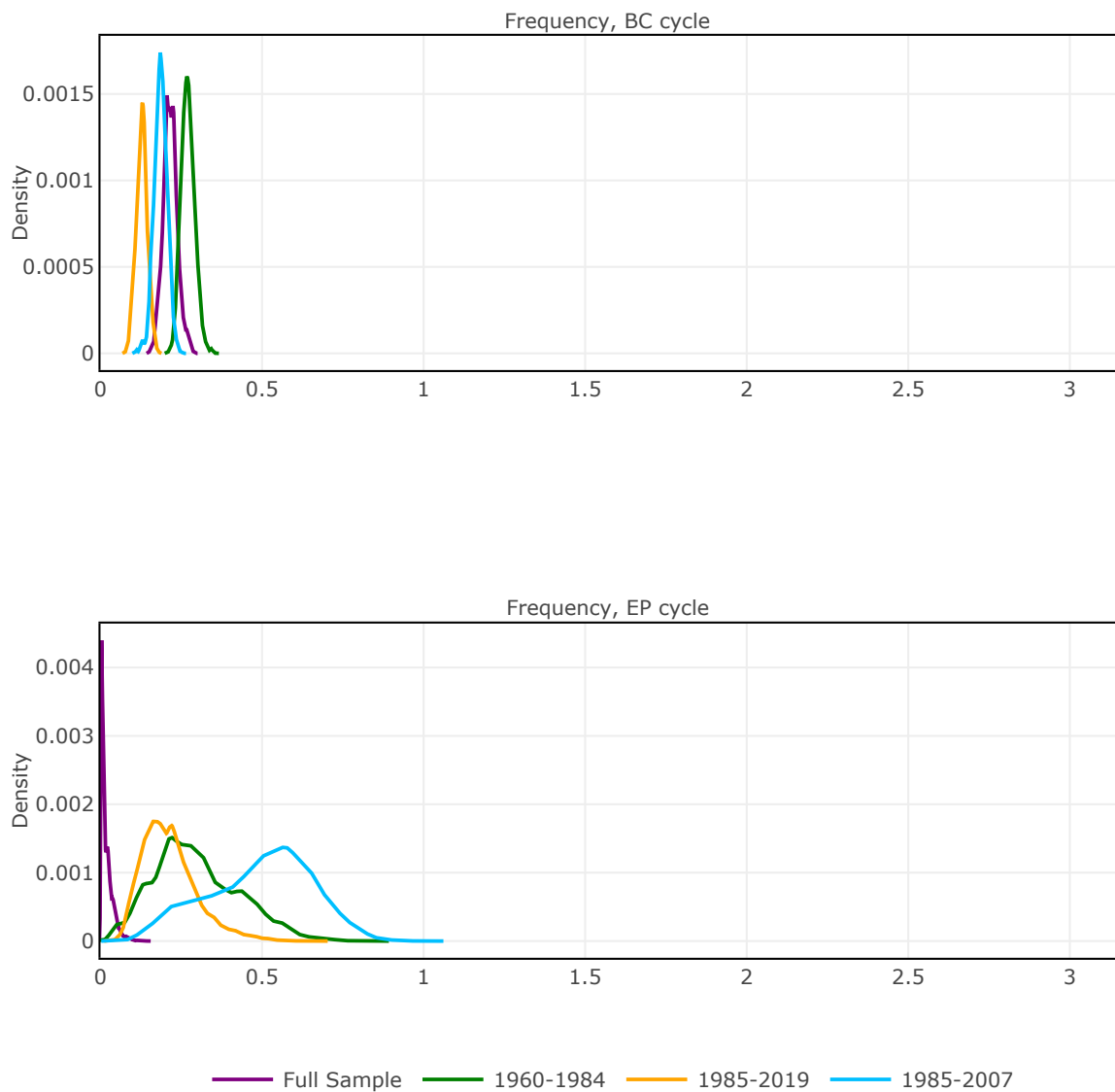


Figure 26: Frequency cycles

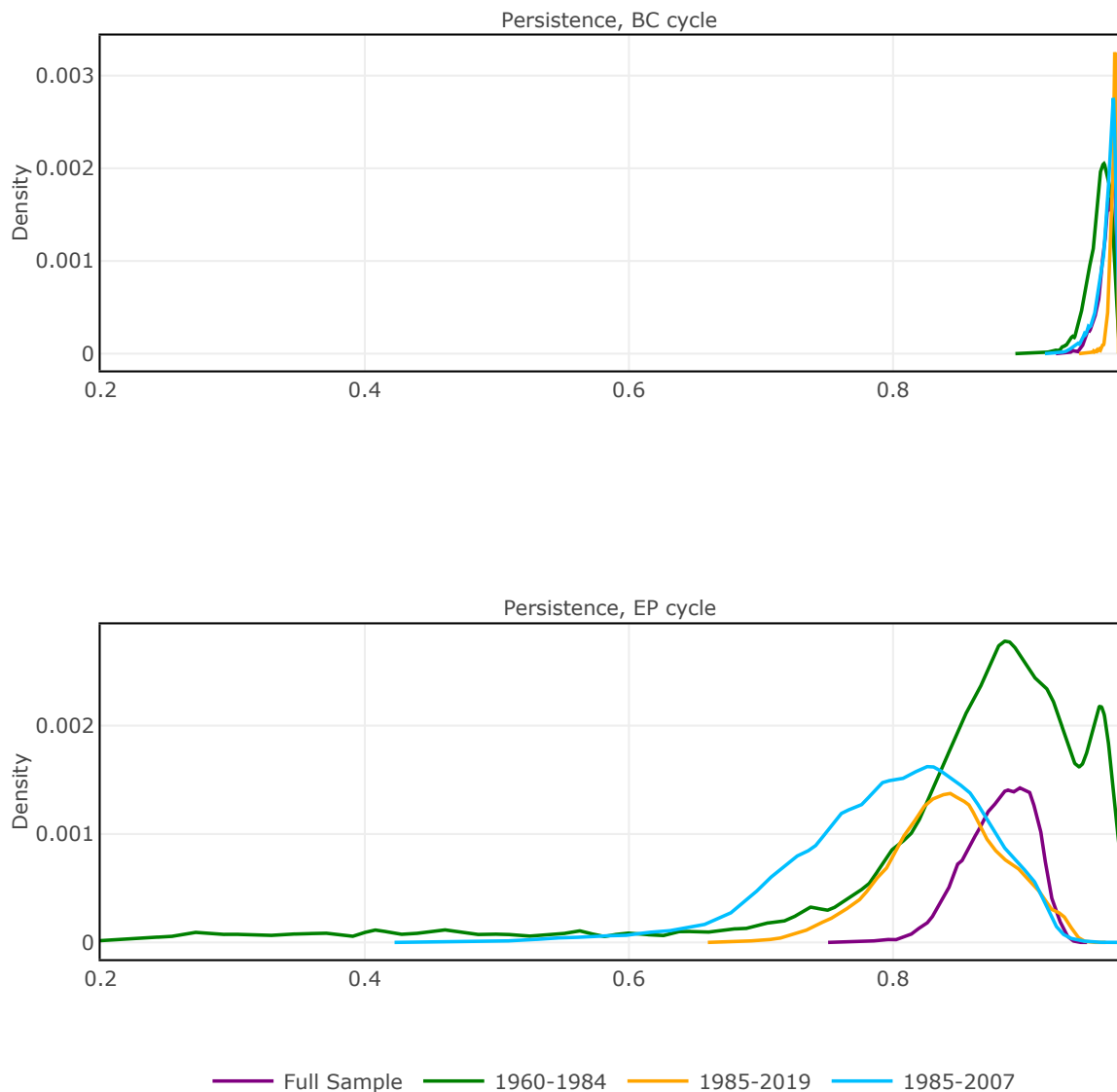


Figure 27: Persistence

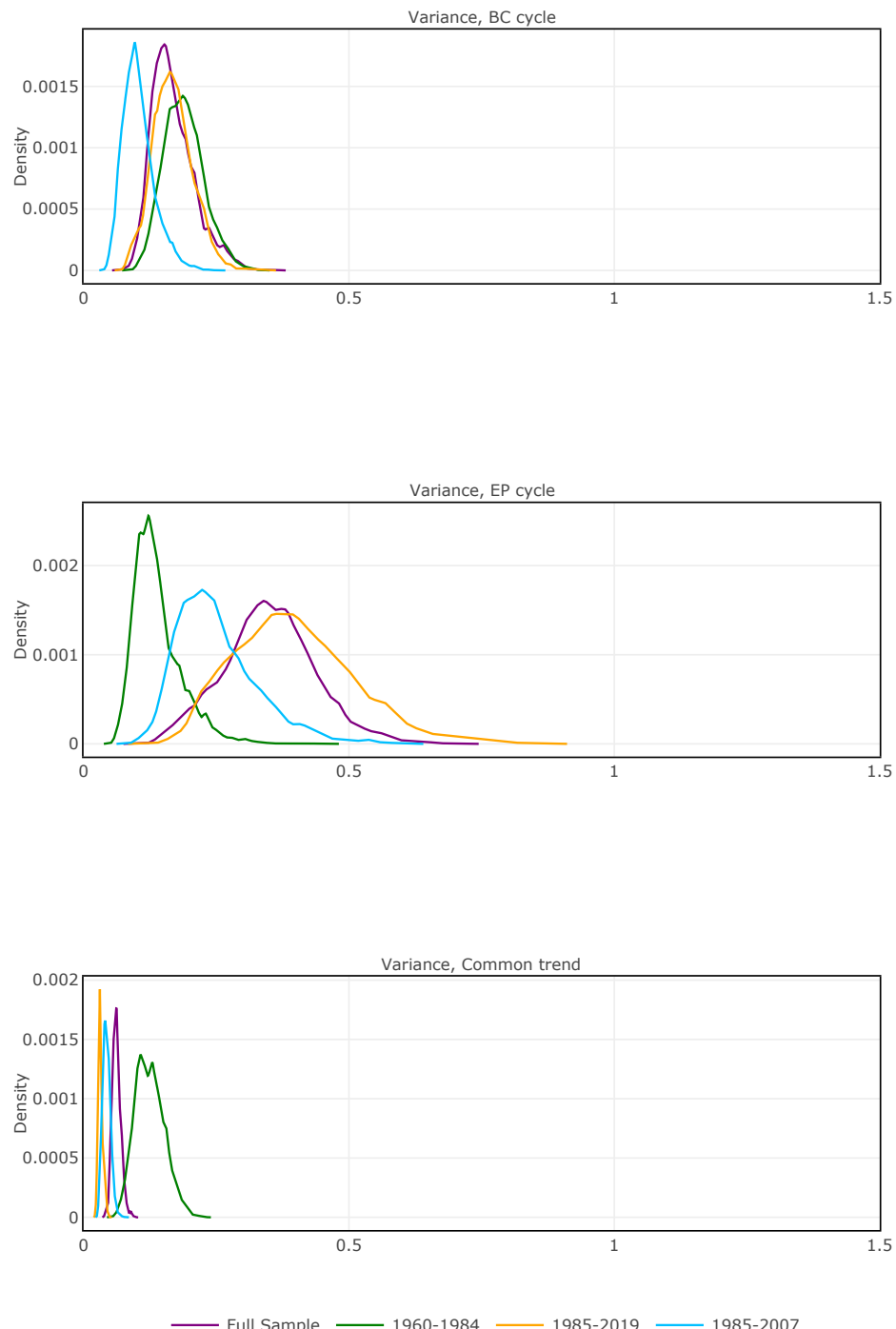


Figure 28: Variance

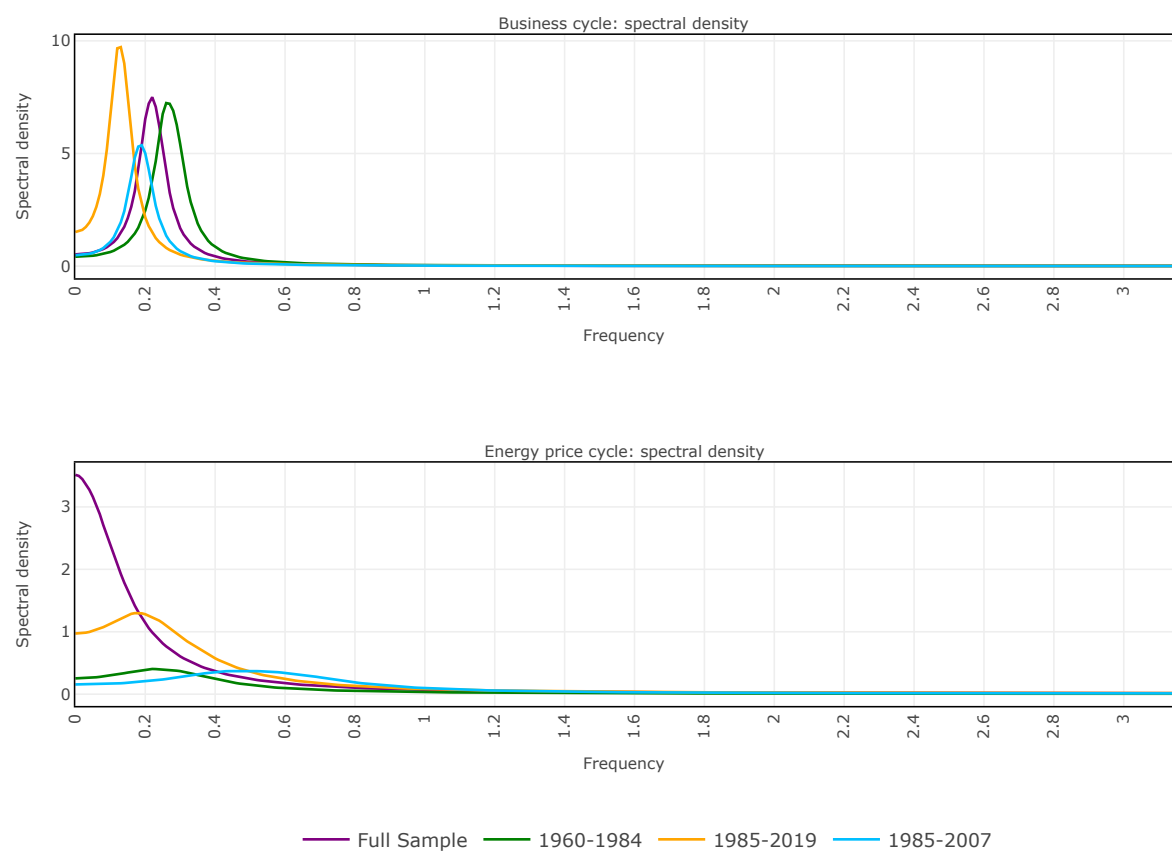


Figure 29: Cycles spectra

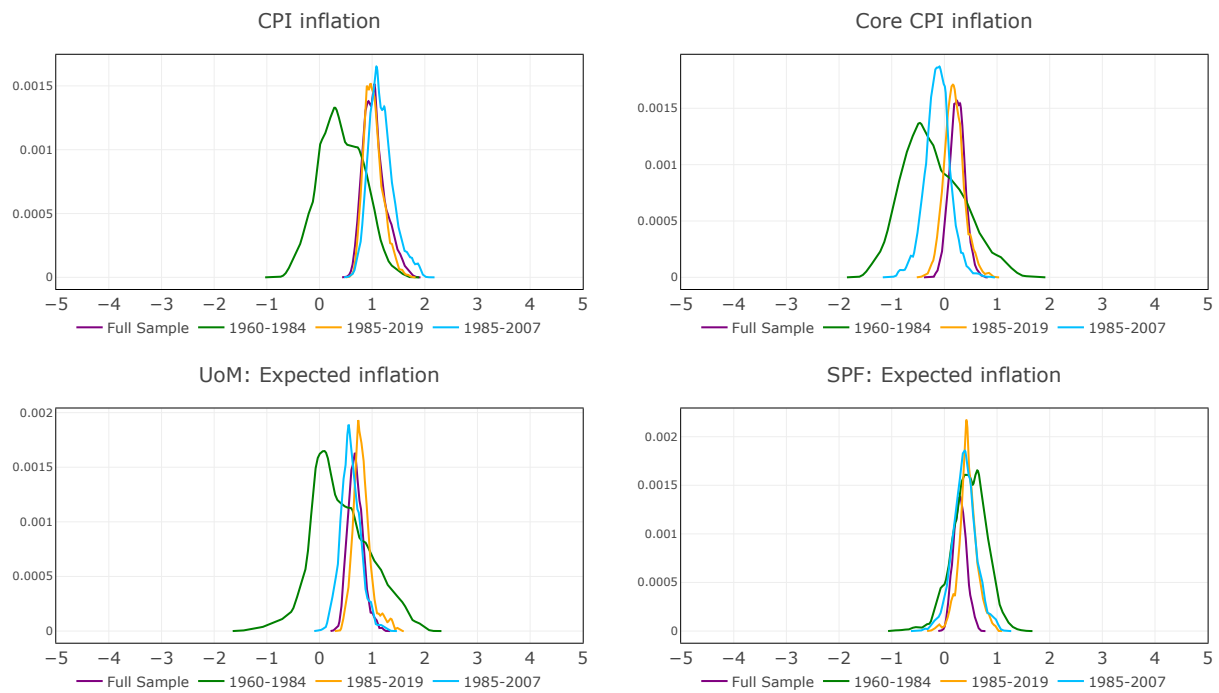


Figure 30: Loadings EP cycle

C Rolling windows

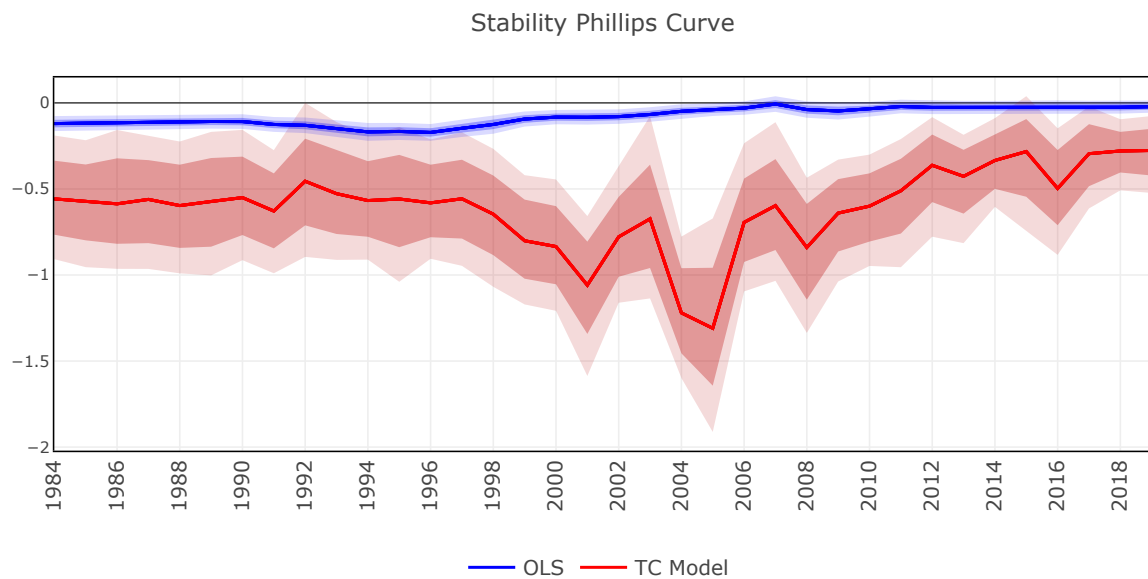


Figure 31: Stability Phillips Curve

D Adaptive Metropolis-Within-Gibbs

D.1 Algorithm

The estimation algorithm is an improved version of the Metropolis-Within-Gibbs in Hasenzagl et al. (2022) that employs the Single Component Adaptive Metropolis proposed in Haario et al. (2005).

This hybrid algorithm is structured in two blocks: (1) a Single Component Adaptive Metropolis (Haario et al., 2005) step for the estimation of the state-space parameters, (2) a Gibbs sampler (Koopman and Durbin, 2000; Jarociński, 2015) to draw the unobserved states conditional on the model parameters. Since we have non-stationary unobserved states, we use the Kalman filter with exact diffuse initial conditions (Koopman and Durbin, 2000; Durbin and Koopman, 2012) to compute the log-likelihood of the model. Finally, we used the priors in Hasenzagl et al. (2022).

Algorithm: Adaptive Metropolis-Within-Gibbs

- **Initialisation**

Let $\mathcal{K} := \{1, \dots, n_k\}$ and denote as $\mathbf{P}(\mathcal{K})$ a function that returns a random permutation of \mathcal{K} (uniformly taken from the full set of permutations of \mathcal{K}). Let also $\boldsymbol{\theta}_0$ be a n_k dimensional vector corresponding to the initial value for the Metropolis parameters. This vector is associated to a high posterior mass.

- **Single component adaptive metropolis**

```
let  $m = 1$ 
```

```
for  $j = 1, \dots, 10000$ 
```

```
let  $\mathbf{S}_j = \mathbf{P}(\mathcal{K})$ 
```

for each k in \mathbf{S}_j

1. *Adaptation:* Update the standard deviation of the proposal distribution

$$\sigma_{k,j} = \begin{cases} 1 & \text{if } j \leq 10, \\ \exp(\alpha_{k,j-1} - 0.44)\sigma_{k,j-1} & \text{otherwise,} \end{cases}$$

where $\alpha_{k,j-1}$ is the acceptance rate for the iteration $j - 1$, for the parameter at position $S_{k,j}$. Besides, 44% is the standard target acceptance rate for single component Metropolis algorithms.

2. *New candidate:* Generate a candidate vector of parameters $\boldsymbol{\theta}_m^*$ such that

$$\theta_{l,m}^* = \begin{cases} \theta_{l,m-1} & \text{if } l \neq k, \\ \underline{\theta} \stackrel{iid}{\sim} \mathcal{N}(\theta_{l,m-1}, \sigma_{k,j}) & \text{otherwise,} \end{cases}$$

for $l = 1, \dots, n_k$.

3. *Accept-reject:* Set

$$\boldsymbol{\theta}_m = \begin{cases} \boldsymbol{\theta}_m^* & \text{accept with probability } \eta_m, \\ \boldsymbol{\theta}_{m-1} & \text{reject with probability } 1 - \eta_m, \end{cases}$$

where

$$\eta_m := \min \left(1, \frac{p[\mathbf{Y} | \mathbf{f}(\boldsymbol{\theta}_m^*)^{-1}] p[\mathbf{f}(\boldsymbol{\theta}_m^*)^{-1}] J(\boldsymbol{\theta}_m^*)}{p[\mathbf{Y} | f(\boldsymbol{\theta}_{m-1})^{-1}] p[\mathbf{f}(\boldsymbol{\theta}_{m-1})^{-1}] J[\boldsymbol{\theta}_{m-1}]} \right),$$

\mathbf{f} and J are defined below.

4. *Increase counter:* Increase m by one.

- **Gibbs sampling**

For $j > 5000$ (burn-in period), use the univariate approach for multivariate time series of [Koopman and Durbin \(2000\)](#) to the simulation smoother proposed in [Durbin and Koopman \(2002\)](#) to sample the unobserved states, conditional on the parameters. In doing so, we follow the refinement proposed in [Jarociński \(2015\)](#).

- **Burn-in period**

Discard the output of the first $j = 1, \dots, 5000$ iterations.

- **Jacobian**

As in [Hasenzagl et al. \(2022\)](#) most parameters are bounded in their support (e.g. the variance parameters must be larger than zero). In order to deal with this complexity, this manuscript transforms the bounded parameters (Θ) so that the support of the transformed parameters (θ) is unbounded. Indeed, the Adaptive Metropolis-Within-Gibbs draws the model parameters in the unbounded space. At a generic iteration j , the following transformations have been applied to a generic parameter i with a Normal, Inverse-Gamma or Uniform prior:

$$\theta_{i,j}^N = \Theta_{i,j}^N$$

$$\theta_{i,j}^{IG} = \ln(\Theta_{i,j}^{IG} - a_i)$$

$$\theta_{i,j}^U = \ln \left(\frac{\Theta_{i,j}^U - a_i}{b_i - \Theta_{i,j}^U} \right),$$

where a_i and b_i are the lower and the upper bounds for the i -th parameter. These

transformations are functions $f(\Theta) = \theta$, with inverses $f(\theta)^{-1} = \Theta$ given by:

$$\Theta_{i,j}^N = \theta_{i,j}^N$$

$$\Theta_{i,j}^{IG} = \exp(\theta_{i,j}^{IG}) + a_i$$

$$\Theta_{i,j}^U = \frac{a_i + b_i \exp(\theta_{i,j}^U)}{1 + \exp(\theta_{i,j}^U)}.$$

These transformations must be taken into account when evaluating the natural logarithm of the prior densities by adding the Jacobians of the transformations of the variables:

$$\begin{aligned} \ln \left(\frac{d\Theta_{i,j}^N}{d\theta_{i,j}^N} \right) &= 0 \\ \ln \left(\frac{d\Theta_{i,j}^{IG}}{d\theta_{i,j}^{IG}} \right) &= \theta_{i,j}^{IG} \\ \ln \left(\frac{d\Theta_{i,j}^U}{d\theta_{i,j}^U} \right) &= \ln(b_i - a_i) + \theta_{i,j}^U - 2 \ln(1 + \exp(\theta_{i,j}^U)). \end{aligned}$$

References

- DURBIN, J. AND S. J. KOOPMAN (2002): “A simple and efficient simulation smoother for state space time series analysis,” *Biometrika*, 603–615.
- (2012): *Time series analysis by state space methods*, vol. 38, OUP Oxford.
- HAARIO, H., E. SAKSMAN, AND J. TAMMINEN (2005): “Componentwise adaptation for high dimensional MCMC,” *Computational Statistics*, 20, 265–273.
- HASENZAGL, T., F. PELLEGRINO, L. REICHLIN, AND G. RICCO (2022): “A Model of the Fed’s View on Inflation,” *The Review of Economics and Statistics*, 104, 686–704.
- JAROCIŃSKI, M. (2015): “A note on implementing the Durbin and Koopman simulation smoother,” *Computational Statistics & Data Analysis*, 91, 1–3.
- KOOPMAN, S. J. AND J. DURBIN (2000): “Fast filtering and smoothing for multivariate state space models,” *Journal of Time Series Analysis*, 21, 281–296.